*International Journal of Fluid Dynamics* (2001) **Vol 5**, Article 2, 17–30
Available online at: http://elecpress.monash.edu.au/ijfd

# Numerical Simulation of the Transition in Three-Dimensional Rotating Flows with Walls: Boundary Layers Instability

E. Serre, P. Bontoux & R. Kotarba
*Lab. Modélisation Simulation Numérique en Mécanique, FRE 2405 CNRS*
*La Jetée IMT Château-Gombert, 38 rue F. Joliot-Curie*
*13451 Marseille Cedex 20, FRANCE*
*email for correspondence: serre1@l3m.univ-mrs.fr*

**Keywords:** Rotating Flows, Direct Numerical Simulation, Instability, Transition

The purpose of this article is the direct numerical simulation (DNS) of the complex phenomena that precede the transition to turbulence inside a cavity subjected to rotation. The configurations of cylindrical cavities subjected to a radial throughflow or to a differential rotation of the walls are relevant to rotating machinery devices. At a high rotation rate, the DNS exhibits instability patterns arising inside the thin layers close to the disks. The efficient spectral solver is based on a Chebyshev-Fourier approximation. For large aspect ratio and at high Reynolds number, an instability occurs inside the Ekman and Bödewadt layers in the form of annular and spiral vortices that are characteristic of type I and type II instabilities.

## 1. INTRODUCTION

The study of rotating viscous flow near stationary or rotating disks has significant relevance to many applications for industrial devices. Many applications have motivated studies involving complex geometries, often with throughflow and heat transfer. Fundamental investigations that are relevant to the cooling of gas turbines and turbomachinery are reported in a series of papers by Owen and Rogers (1989, 1995). In the limit of high rotation rate, the flow between a rotating and a stationary disk presents two boundary layers, an Ekman layer on the rotating disk and a Bödewadt layer on the stationary disk, separated by a geostrophic core.

Two basic types of instability for corotation of the fluid and the disk have been documented experimentally and theoretically. Historically these are referred to as type I (or type B) and type II (or type A) instabilities. The type I instability (or "cross flow" instability) is associated with an inflection point in the profile of the normal velocity with respect to the disk plane (here, the radial velocity profile), whereas the type II instability, appearing at lower values of the critical Reynolds number, is related to the combined effects of the Coriolis forces and viscosity (Lilly 1966). The spatial structure of both instabilities consists of travelling vortices in the boundary layers. Their wavelength depends on the boundary

layer thickness (about $10\delta$ and $20\delta$ for type I and type II, respectively, where $\delta = 0.5(\Omega/\nu)$ and $\Omega$ and $\nu$ are defined in the following section) and the orientation of their wave fronts with respect to the geostrophic flow (positive for the type I instability and negative for the type II instability).

Linear stability analyses of the flow between a rotating and a stationary disk predict several instabilities, based on similarity solutions for the base flow (San'kov and Smirnov 1991) and the stability of Batchelor-type solutions with a separated boundary layer, i.e., for high rotation rates (Itoh 1991). The critical values found by these authors do not agree, and the mechanisms for the instability are not clear. We also note the results of the stability analysis for Ekman-Couette flow with two Ekman boundary layers by Hoffman *et al.* (1998). In this configuration two parallel plates move relative to each other with a constant velocity in a system that rotates with an angular velocity normal to the plates. This study predicts a steady roll instability for a low rotation rate and instabilities of type I and type II for increasing rotation rates. In a later study on the same Ekman-Couette flow, Hoffman *et al.* (2000) found an isolated solution describing a solitary vortex wave which does not seem to bifurcate from any other known solution. This solution is critical in a range of moderate rotation rates below the onset of the type I instability, but is unstable with respect to three-dimensional disturbances.

Experimental studies on the stability of the Ekman layer (Faller 1963, Caldwell and Van Atta 1970) and others (see Crespo del Arco *et al.* 1996 for an extensive bibliography) have investigated the type I and type II instabilities. The three-dimensional rolls found in experiments have characteristic parameters (angle, phase velocity, and wavelength) that are in reasonably good agreement with linear stability predictions. Savas (1987) studied experimentally unsteady uniformly rotating flow over a stationary disk and observed both type I and type II instabilities during the nonlinear phase of spin-down. Savas noticed the presence of both ring and spiral structures. In both the rotor/stator cavity and in the Ekman layer on a single disk, the experimental results exhibit similar spatial structures.

The evolution of the aforementioned types of flow and higher bifurcations have received relatively less attention in the literature. The experimental studies of Schouveiler *et al.* (1996, 1998, 1999) present the evolution and further transitions of the flow regimes for a wide range of the geometrical and control parameters. They report a variety of instability patterns depending on the aspect ratio of the cavity. For a basic state of Batchelor-type flow, the critical instability has the form of annular rolls and spiral waves with positive angles developing for increasing rotation rate. When the basic state is a viscous flow—that is when the two boundary layers merge at high rotation rate—the critical instability consists of spiral rolls with negative angles. In addition, structures without spatial or temporal periodicity (such as solitary waves or spots) were observed far from the axis during the transition to turbulence (see also San'kov and Smirnov 1984).

More details concerning the throughflow and the rotor-stator cavities related to these problems are described by Serre *et al.* (2001), and Serre & Pulicani (2001).

In this work, a wide range of flows driven by the differential rotation of the walls and by a throughflow are presented. These flows are simulated with an efficient three-dimensional spectral method. The characteristic parameters of the solution such as wavelength, phase velocity and angle of spiral arms are related to the available theoretical and experimental results for type I and type II instabilities.

## 2. MODELS

### 2.1. GEOMETRIC MODELS

The geometric models correspond to two annular disks, where $R_0$ and $R_1$ are the inner and outer radii (Figures 1a and b). In the case of a cylindrical cavity, the inner radius is $R_0 = 0$ (Figure 1b). The domain can be open to permit radial outflow boundary conditions (Figure 1c), or completely enclosed by one (Figure 1b) or two cylinders of height $2h$ (Figure 1a), corresponding to an internal shaft and an external shroud. The disks in the open cavity rotate at the same angular velocity (Figure 1c). The enclosed cavities have a stationary disk (stator) and a disk (rotor) rotating at angular velocity $\Omega$ (Figures 1a and b).

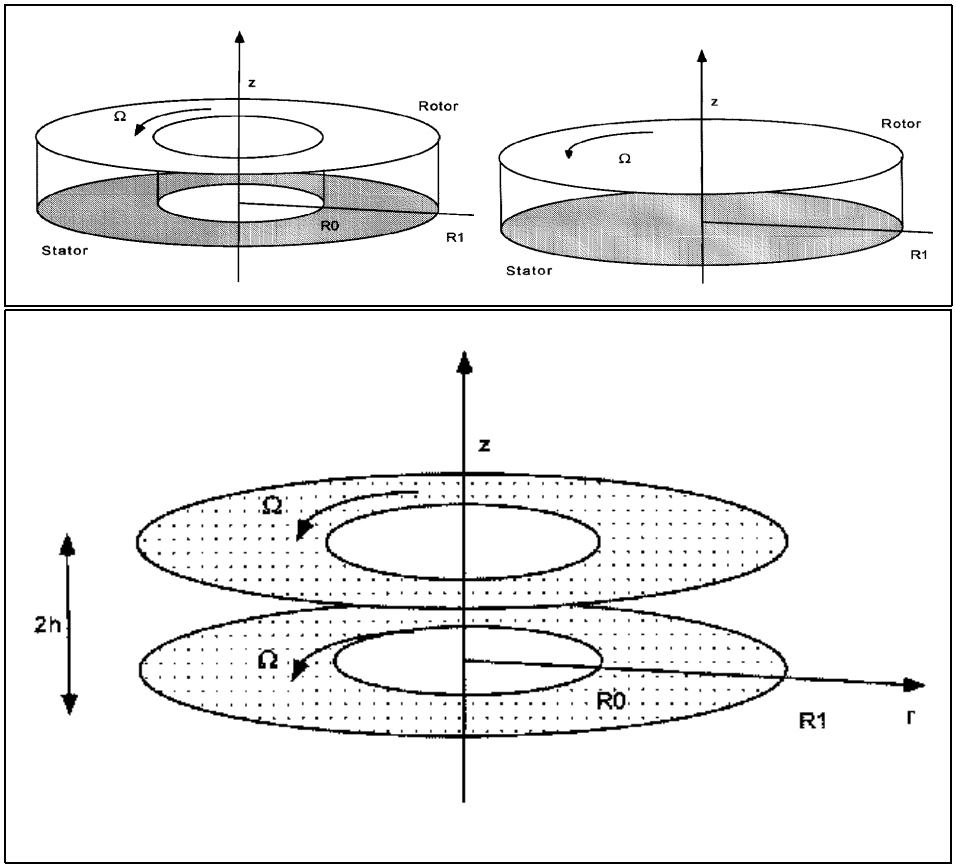


Figure 1. Geometric models. (a) Top left: annular rotor-stator cavity, (b) Top right: cylindrical rotor-stator cavity ($R_0 = 0$), (c) Bottom: rotating annular cavity with a radial outflow.

### 2.2. MATHEMATICAL MODEL

The fluid motion is governed by the three-dimensional incompressible Navier-Stokes equations written in primitive variables. Two geometrical parameters define the curvature and

the aspect ratio, $R_m = (R_1 + R_0)/\Delta R$ and $L = \Delta R/2h$, where $\Delta R = R_1 - R_0$. In the case of the cylindrical cavity $R_m = 1$ and $L = R_1/2h$. The scales for non-dimensionalizing space, time and velocity are $[h, \Omega^{-1}, \Omega R_1]$, respectively. The dimensionless components of the velocity vector are ($u$, $v$, $w$) in the radial, azimuthal and axial direction and $p$ is the dimensionless pressure. The dimensionless radial and axial spatial variables are denoted ($r'$, $z'$). The use of Chebyshev polynomials requires these variables to be normalized to have values between [-1, 1]. Thus, the normalized spatial variables are denoted ($r$, $z$) where $r = (2h/r' - R_0 - R_1)/\Delta R$ and $z = z'$.

The relevant physical parameters are the Reynolds number, defined by $Re = \Omega h^2/\nu$ where $\nu$ is the kinematic viscosity of the fluid and, when a radial outflow is imposed, the mass flow rate, $Q$, made dimensionless as $C_w = Q/\nu R_1$. For radial outflow, the flow is forced from $R_0$ to $R_1$ parallel to the plane of the disks.

#### 2.2.1. *Boundary Conditions*

In all cases, the boundary conditions correspond to no-slip conditions for $u$ and $w$ at the rigid walls. For the open cavity, an Ekman boundary layer flow (Hide 1968) is assumed at $R_0$ and $R_1$. For the cylindrical rotor-stator cavities, the boundary conditions for the azimuthal velocity component are the same as for physical devices: $v = 0$ on the stationary portion, and $v = (R_m + r)/(R_m + 1)$ on the rotating top disk. The junction between the stationary cylinder and the rotor involves a singularity in the azimuthal velocity. This singularity corresponds to a physical situation where there is a thin gap between the edge of the rotating disk and the stationary sidewall. We have retained this condition in the "cylindrical" model since it is relevant to physical devices. In the "annular" model, the boundary conditions have been modified using a virtual wall that incorporates a linear azimuthal velocity profile between the disks at $R_0$ and $R_1$, as previously proposed by Cousin-Rittemard *et al.* (1998). This linear profile is interesting from a mathematical point of view because it reduces sources of error that could affect the numerical solution. The two-dimensional results of these authors provide benchmark solutions for our computations. They were the first to bring an explanation of the phenomenon of the direct transition from a steady to a time-dependent "chaotic" boundary layer attributable to curvature and confinement effects. For the range of parameters $(L, Re)$ considered in this work, Serre *et al.* (2001) have shown that similar patterns are nevertheless obtained with both the actual (discontinuous) and the modified linear velocity profile boundary conditions. Only slight differences (at the same Reynolds number) occur near the shroud region but do not affect the boundary layer of the stationary disk. At the shaft and at the shroud, a continuous variation is considered of the form $v = (1 + z)(R_m + r)/2(R_m + 1)$, $r = \pm 1$.

### 2.3. NUMERICAL MODEL

The numerical solution is based on a pseudo-spectral collocation Chebyshev-Fourier Galerkin method. The use of the Gauss-Lobatto collocation points in the radial and axial directions directly ensures high accuracy of the solution inside the very narrow wall layers. The time scheme is semi-implicit second-order accurate. It corresponds to a combination of the second-order backward differentiation formula for the viscous diffusion term and the Adams-Bashforth scheme for the nonlinear terms. The velocity-pressure coupling is performed with a improved projection algorithm (Serre and Pulicani 2001). A dependent

variable transformation is introduced in order to deal with the lack of a physical boundary condition at the axis in the case of the first Fourier axisymmetric mode as proposed by Serre and Pulicani (2001).

Different grids are used depending to the value of the Reynolds number $Re$ (rotor-stator cavity) or the mass flow parameter $C_w$ (open rotating cavity) and of the curvature parameter $R_m$: $48 \times 48, 64 \times 64, 123 \times 123$ and $152 \times 152$ in $(r,\, z)$ plane with from 48 to 128 Fourier modes in the azimuthal direction. The grid refinement corresponds to the need to resolve the nonlinear effects. The time-steps employed are $\Delta t = 4 \times 10^{-3}$, $2 \times 10^{-3}$ and $10^{-3}$ (for both high resolution grids) and correspond to a compromise between the stability criterion of the numerical method and the time scale of the physical phenomenon.

Refinement studies and time-step effects were tested in the rotor-stator cavity ($R_m = 5$) at $Re = 330$. The solutions are grid and time-step independent: the space and time scales of the instability differ by less than 0.1% with changes in the grid spacing and time-step. Moreover, previous axisymmetric studies of a rotating annular cavity (Crespo del Arco *et al.* 1996) indicate that spatial resolutions of $48 \times 48$ and $64 \times 64$ in $(r, z)$, for $Re = 330$, $R_m = 5$ and for $C_w = 530$, provide a good compromise between required accuracy and computational cost.

For the time-dependent solutions, the computing time depends on the largest characteristic time in rotating flows, i.e., the viscous time $\tau_\nu = h^2/\nu$ (Greenspan 1969). The dynamic behavior of the variables is analyzed at several key locations in each layer and in the core. The radial wavelength is defined as $\lambda_r = \Delta R/n$, where $n$ is the number of pairs of vortices along the radius. This number is estimated from displayed contours of the axial component of the velocity $w$ or from the fluctuation (for the rotor-stator configuration), taking into account the side wall effects. A pair of rolls corresponds to the distance between two successive extrema of same sign. The wavelength is sized in terms of the length scale of the Ekman layer $\delta$, as is typical in the literature. A local Reynolds number is also defined as $Re_\delta = \Omega \delta r^*/\nu$ where $r^*$ is the dimensional radius.

## 3. RESULTS AND DISCUSSION

### 3.1. ROTOR-STATOR CAVITY

The cases of the annular cavity with aspect ratio $L = 5$ and curvature parameters $R_m = 4$ and $R_m = 5$ correspond to radial variable $r' \in [15, 25]$ and $r' \in [20, 30]$, respectively. For the cylindrical configuration, the aspect ratio is $L = 2$ corresponding to $r' \in [0, 4]$ and $L = 5$ corresponding to $r' \in [0, 10]$.

#### 3.1.1. *Axisymmetric annular instabilities*

Two kinds of axisymmetric instabilities have been computed starting from the stationary basic flow. The first one is a stationary instability on the Bödewadt layer, characterized by 3 pairs of circular rolls ($6 < \lambda_r/\delta < 11$) and which is observed (for the first time numerically) in the annular cavity for $Re = 330$. This stationary axisymmetric solution has very similar characteristics to the experiments of Sirivat (1991) for a cylindrical cavity of $L = 10.52$ and for $Re = 88.6$. These experiments showed stationary circular rolls of wavelength $9.4 < \lambda_r/\delta < 14$ that are related to the type II instability of the Bödewadt layer, quite similar to our present simulations.

When the rotation rate is increased further, the instability is time-dependent in both the annular cavity $R_m = 4$ and the cylindrical cavity $L = 2$.

- In the annular cavity for $Re = 400$, the solution is oscillatory with a fundamental angular frequency $\sigma = 4.7$ ($\sigma = 2\pi f$). The axisymmetric vortices are visible along the two layers on both disks and travel with the flow. Inside the Ekman layer, 3 pairs of large circular rolls, $19.5 < \lambda_r/\delta < 30$, arise whereas in the Bödewadt layer, the solution exhibits about 5 pairs of counter-rotating rolls ($11 < \lambda_r/\delta < 17.6$). The vortices move with a radial phase velocity $V_\phi = \lambda_r\sigma/2\pi$, which decreases slightly with the radial location such that $0.08 < V_\phi/\Omega r^* < 0.12$. Recent experiments by Gauthier *et al.* (1999), and Schouveiler *et al.* (1999) report similar oscillatory axisymmetric patterns in a cylindrical cavity but far from the axis. Typically, they found the angular frequency and wavelength are $\sigma = 4$ and $\lambda_r/\delta = 25.4$ at$Re = 128$ for a cavity of large aspect ratio $L = 10.45$.
- In the cylindrical cavities, the axisymmetric instabilities appear for $Re = 4000$ for $L = 2$, and $Re = 1600$ for $L = 5$. Unlike the annular cavity, the Ekman layer on the rotating disk remains stable. For $L = 2$, $Re = 4000$, a Hopf bifurcation to a periodic oscillatory solution ($\sigma = 0.9$, close to the rotation frequency of $\sigma = 1$) occurs in agreement with the observations of Cousin-Rittemard *et al.* (1998). This solution is characterized by 4 to 5 pairs of vortices ($10 < \lambda_r/\delta < 21$) that develop as annular structures. These vortices appear at the external wall (stationary in this configuration) and travel slowly inward ($0.02 < V_\phi/\Omega r^* < 0.08$) in the Bödewadt layer down to $r' = 0.5$ near the axis corresponding to a local Reynolds number of $Re_\delta = 21$. For a larger aspect ratio $L = 5$, we did not observe a transition to time-dependent flow via a Hopf bifurcation (probably due to confinement), but the solution is oscillatory with the dominant frequency nearly $\sigma = 4$. This solution is characterized by vortices ($8 < \lambda_r/\delta < 25$) that vanish at distance $Re_\delta = 27$ from the axis. The latter results in cylindrical cavities are quite similar to the experimental results of Savas (1987) for a cavity of aspect ratio $L = 0.5$. In this case, traveling circular waves were observed during an impulsive spin-down for $25 < Re_\delta < 125$, where $Re_{\delta_c} = 25$ is a critical Reynolds number very close to those in our simulations; $Re_{\delta_c} = 21$ for $L = 2$ and $Re_{\delta_c} = 27$ for $L = 5$. Savas observed about 9 pairs of rolls ($10.5 < \lambda_r/\delta < 31$) evolving inward with an estimated phase velocity of about $V_\phi/\Omega r^* = 0.135$ decreasing slightly towards the center $V_\phi/\Omega r^* = 0.093$. The frequency $\sigma = 5$ given by Savas (1987) is close to $\sigma = 4.76$ computed for $R_m = 4$, $L = 5$ further from the axis in the annular cavity but five times larger than $\sigma = 1$ computed near the axis. Schouveiler *et al.* (1999) found axisymmetric structures that travel inward with an angular frequency decreasing from $\sigma = 3$ (in a region close to the external wall) down to $\sigma = 1$ near the axis, in a zone similar to the computational domain in the cylindrical cavity. This behavior is attributed to dislocation phenomena during which periodic pairings of two vortices is observed. In all these axisymmetric cases we have not observed this pairing effect of the circular vortices as they travel over the radius of the cavity as was found in recent experiments by Gauthier *et al.* (1999).

Thus, the present computed values of characteristics ($\lambda_r$, $\sigma$, $V_\phi$) are in good agreement with previous experimental and numerical results. Thus, following the analysis of Savas (1987), the instabilities are of type II in both the Bödewadt and the Ekman layers.

3.1.2. *Three-dimensional spiral instabilities*

The rolls that progress in the form of rings in the axisymmetric solution, now constitute spirals arms and expand inside the cavity. We notice also the occurrence of coexisting rings and spiral patterns in the Bödewadt layer for $Re = 400$, $R_m = 4$ and for $Re = 1600$, $L = 5$, respectively.

Due to the high level of accuracy of the spectral solution, the truncation error remains very low and due to the precision of the supercomputer (10-16 on a Cray C98), the round-off errors are quite small. Thus, numerical noise is at a very low level. The increase in numerical noise (that should drive the solution to 3D patterns) is very costly in CPU time, so the transition to three-dimensional patterns was accelerated via "artificial" initial disturbances. The general form is $a\sin(p\theta)$ where $p$ is an arbitrary number corresponding to an azimuthal wavelength and $a$ the magnitude (scaled with respect to the azimuthal velocity). A typical value of $a$ is 0.05. The disturbance is superimposed on a previous axisymmetric solution, and introduced locally near the shroud at about $L(R_m + 0.7) < r' < L(R_m + 1.0)$. Identical results are obtained from disturbing the azimuthal velocity or the other components of velocity. The general wavelength of the spiral patterns can be defined as $\lambda = 2pr^*/n\sin\epsilon$, where $n$ is the number of arms over $2\pi$ at dimensional radius $r^*$, and $\epsilon$ is the orientation of the wavefront with respect to the azimuthal direction (it is defined positive when it is rolled up towards the axis of the disk in the rotation direction). We note that the three disturbances (of azimuthal wavelength $\lambda = 2\pi/3$, $2\pi/8$ and $2\pi/12$) give rise to the same three-dimensional solution in the annular cavity. In the cylindrical cavity no computations have been performed for disturbances of different wavelengths.

*3.1.2.1 Pure spiral patterns (unmixed with any circular pattern)*

Pure spirals arise in annular cavities at large distances from the axis ($R_m = 5$) and also in the near axis region of cylindrical cavity where confinement is important ($L = 2$). In the case of the annular cavity ($R_m = 5$, $L = 5$), an oscillatory solution is obtained for the axisymmetric stationary flow at $Re = 330$. The velocity fluctuations with respect to the averaged flow solution display the spatial structure of the instabilities at an instant (Figure 2). The angular frequency is $\sigma = 21.4$ and a spiral structure with $n = 22$ arms arises in both layers. Inside the Ekman layer are 8 pairs of rolls in the radial direction for which the angle of the spiral wavefront decreases with the radius as $-6.9 < \epsilon < -15.3$. The resulting wavelength on the rotating disk diminishes with the radial location over a range $9.4 < \lambda/\delta < 13.8$ and the phase velocity $V_\phi = \lambda\sigma/2\pi$ simultaneously decreases as $0.12 < V_\phi/\Omega r^* < 0.26$. These 3D spiral patterns have been observed experimentally in the Ekman layer (see a review by Faller, 1991). Caldwell and Van Atta (1970) and Faller (1966) found similar structures experimentally for $22 < \lambda/\delta < 33$ and an angle $-20 < \epsilon < 5$ that they referred as the type II instability of the Ekman layer. Close to the stationary disk the spatial structure of the vortices has some similarities to those in the rotating disk layer ($14.9 < \lambda/\delta < 20.4$), but the spiral arms form a positive angle, $11 < \epsilon < 23$, that reveals a wider inclination with respect to the geostrophic flow. The spiral wavefront (represented by the arms) travels inward with a phase velocity that varies with the radius as $0.25 < V_\phi/\Omega r^* < 0.28$.

*3.1.2.2 Mixed annular and spiral patterns*

The cylindrical cavity with large aspect ratio $L = 5$ and the annular cavity closer to the

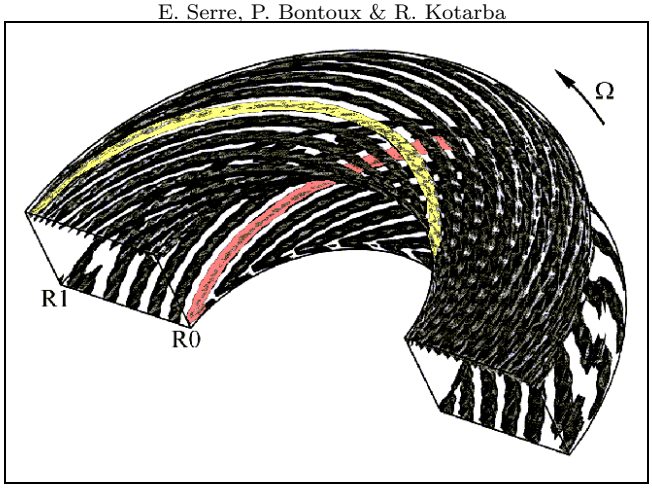


Figure 2. Spiral patterns of the instability in the rotor-stator cavity. Three-dimensional display of iso-surfaces of the fluctuation of the axial velocity component: (a) Ekman and Bödewadt layers instability (yellow and pink arms, respectively) in the annular cavity ($R_m = 5$, $L = 5$), $Re = 330$.

axis ($R_m = 4$, $L = 5$) are now considered to reduce the confinement effect and increase the curvature effect. The spatial structure is more complex (Figure 3). Spiral and annular structures coexist inside the Bödewadt layer and pairing effects occur near the rotating disk in the annular cavity (Figure 3a) and near the stationary disk in the cylindrical cavity (Figure 3b).

- In the annular cavity, the time history reveals two major frequencies in different regions of the cavity for $R_e = 400$. The smaller frequency, $\sigma_2 = 8$, is dominant in the stationary disk layer and the larger one, $\sigma_1 = 16.2$, is dominant in the rotating disk layer. The frequency $\sigma_1$ also dominates at the rotor-shroud corner while both $\sigma_1$ and $\sigma_2$ are of same magnitude at the rotor-shaft and stator-shroud corners. Inside the Ekman layer, there are 7 pairs of rolls in the radial direction and 18 spiral arms having an angle $\epsilon$, that steeply decreases from $R_0$ to $R_1$, in the range $9.4 < \lambda_r/\delta < 14$. The associated wavelength increases in the range $11.4 < \lambda_r/\delta < 17.9$. The vortices evolve outward, with a phase velocity $0.12 < V_\phi/\Omega r^* < 0.30$. The number of arms changes between the shaft at $R_0$ and the shroud at $R_1$ exhibiting a zone with dislocations. These spiral patterns have characteristic parameters ($\lambda$, $e$) very close to the previous ones described for $L = 5$, $R_m = 5$ and are related to type II instability. Inside the Bödewadt layer, 4 pairs of rolls of average radial wavelength $\lambda_r/\delta = 19.2$ develop close to the shaft into 18 spiral arms forming an angle $15.6 < \epsilon < 23$. In addition, two pairs having a larger wavelength $\lambda_r/\delta = 26$ develop in rings close to the shroud. The persisting axisymmetric structures interact with the spiral arms at $r' = 8$ and travel inward with a radial phase velocity $0.19 < V_\phi/\Omega r^* < 0.27$.

The coexistence of these two types of waves was first described during a transient spin-down by Savas (1987) who reported patterns that simultaneously involve spiral waves with 23 arms of positive angle, ranging between 12° and 18° and circular waves. Savas related

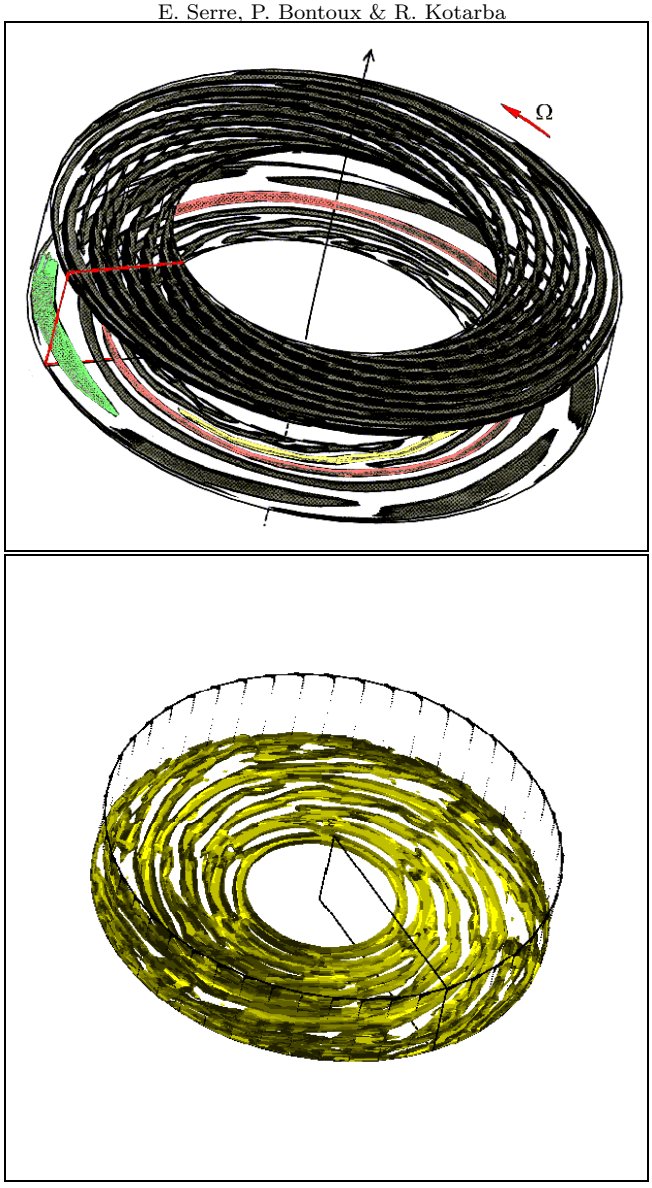


Figure 3. Mixed annular and spiral patterns of the instability in the rotor-stator cavity. Three-dimensional display of iso-surfaces of the fluctuation of the axial velocity component. (a) Top: Ekman and Bödewadt layers instability in the annular cavity ($R_m = 5$, $L = 5$, $Re = 330$). The annular structure is colored pink and the spiral arms are colored in yellow and green close to the shaft. (b) Bottom: Cylindrical cavity ($L = 5$, $Re = 1200$).

these spirals to the type I instability of Bödewadt layer. The axisymmetric structures appeared close to the shroud as in our numerical solution.

- In the cylindrical cavity ($L = 5$), the disturbance is superimposed on the steady axisymmetric solution obtained for $Re = 1200$ and the temporal behavior exhibits an oscillatory regime with a major angular frequency nearly equal to the rotation frequency and very close to the computed one for $Re = 4000$ and $L = 2$. Then 8 pairs of rolls move downstream to $r' = 1.54$ ($Re_\delta = 26.64$) with a phase velocity $0.02V_\phi/\Omega r^* < 0.27$. For $1.54 < r' < 5$ ($26.64 < Re_\delta < 86.5$) the vortices transform to 5 annular structures. At a larger distance from the axis, rolls develop in the form of 6 spiral structures with an angle of $7 < \epsilon < 28$ and exhibit pairing phenomena.

Unlike the previous annular case ($R_m = 4$, $L = 5$) and experiments by Savas (1987), the spiral structures occur close to the shroud at larger local Reynolds number $Re_\delta$ consistent with recent experiments by Schouveiler *et al.* (1999) and Gauthier *et al.* (1999). Thus it seems that these spiral structures correspond to the type I instability of the Bödewadt layer. Nevertheless, we cannot determine from the present results if the coexistence of these two types of structures is a consequence of the confinement effect or if it results from different values of the local parameters revealing two different types of instabilities inside the same layer.

## 3.2. ROTATING CAVITY WITH A RADIAL OUTFLOW

The basic flow is steady and axisymmetric and corresponds to the Ekman layer flow. For this type of flow, the Coriolis force dominates with respect to inertial and centrifugal forces near the walls. The flow organizes itself symmetrically and parallel Ekman layers form on the two disks with the same mass flow rate (Serre *et al.* 2001). In all cases the Reynolds number is $Re = 1750$. In the numerical solutions, the meridional $(r, z)$ flow concentrates near these two Ekman layers while outside, in the geostrophic core, the Coriolis force balances the pressure force and the flow is primarily azimuthal.

### 3.2.1. *Axisymmetric annular instabilities of the basic flow*

When increasing the mass flow rate to $C_w = 530$ (from the stable solution at $C_w = 460$), the flow is axisymmetric and oscillatory with an angular frequency $\sigma = 7.4$. The computed value of $\sigma$ and the frequency reported from experiments by Caldwell and Van Atta (1970) far from the critical Reynolds number agree quite well. In the numerical solution six pairs of counter-rotating axisymmetric rolls ($\lambda_r = 24\delta$), slightly decreasing from $26\delta$ to $23\delta$ between $R_0$ and $R_1$, occur in the Ekman layer over the radial extent, travelling radially outward with a phase velocity of about $V_\phi/V_g = 0.28$ (Figure 4), where $V_g$ is the geostrophic velocity (azimuthal component of the velocity in the inviscid core). Good agreement with the theoretical results is obtained. The range of the parameters ($\lambda_r$, $\sigma$, $V_\phi$) is characteristic of the axisymmetric mode of the type II Ekman boundary-layer instability.

### 3.2.2. *Three-dimensional finite-amplitude instabilities*

The same disturbance that superimposed in the rotor-stator case is used near the entrance section. Disturbances of different amplitudes are shown to give exactly the same spiral flows but the transient time to reach the stable state noticeably depends on $a$. In this case, we have estimated the transient time by perturbing the same nonlinear Ekman axisymmetric solution with various amplitude rates $a = 0.8\%$, $2\%$ and $5\%$. The results indicate that the transient

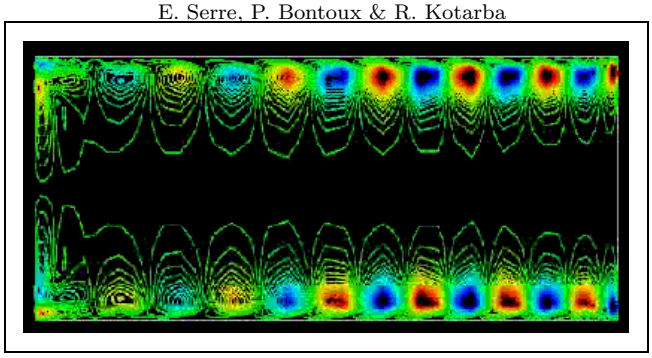

Figure 4. Axisymmetric time-dependent instability in the annular rotating cavity ($R_m = 5$, $L = 3.37$) for $Re = 1750$ and $C_w = 530$. Iso-lines of the fluctuation of the axial velocity in the plane ($r$, $z$, $\pi/4$). Animation available on the IJFD website.

behaves roughly as $a^{-1/3}$ (Serre *et al.* 2000). We obtain multiple periodic solutions with different numbers of spiral arms dependng on the periodicity of the disturbances (Figure 5, the solution with 12 spiral arms in the Ekman layer). These solutions are stable to further disturbances. The characteristics of the stable solutions at the center of the cavity are given in Table I.

| Number of arms, $n$ | $p$ | $\sigma$ | $\epsilon$ (deg) | $\lambda/\delta$ | $V_\phi/V_g$ |
|---|---|---|---|---|---|
| 0 | - | 7.4 | 0 | 0 | 0.28 |
| 6 | 3,6 | 8.55 | -3.64 | 23.68 | 0.32 |
| 7 | 7 | 8.73 | -4.25 | 23.69 | 0.32 |
| 8 | 2,4,6 | 8.98 | -4.85 | 23.65 | 0.33 |
| 12 | 4,12 | 9.86 | -7.26 | 23.57 | 0.36 |
| 14 | 14 | 10.24 | -8.45 | 23.49 | 0.38 |

Table I: Characteristics of the different stable solutions for $Re = 1750$, $Cw = 530$.

We can observe that the angular frequency increases with the number of arms, $\sigma \gg n$. Moreover, a generic equation of the wavefront can easily be derived from the condition of colinearity between the displacement of the instability and the phase velocity. Using the present results we can determine an equation of the wavefront as:

$$r^2 = \frac{2\pi L R_m}{3\pi}\left(\theta + \frac{2i\pi}{n}\right).$$

The angle of the wavefront with the geostrophic velocity thus varies with $r^{-2}$ according to:

$$\tan\epsilon = -\frac{u}{v} = \frac{nR_m}{6\pi(R_m + r)^2}.$$

These 3D spiral patterns have already been experimentally observed in the Ekman layer (see a review by Faller, 1991, and by Crespo del Arco *et al.,* 1996) and the characteristic parameters are in good agreement with those obtained in the relevant experiments (Caldwell and Van Atta 1970; Faller 1966). Moreover, the present results are quite similar to those given by the stability analyses in the case of an infinite disk (Faller 1991). Thus, the spiral structure of the computed rotor layer shows the same characteristics as the standard type II instability of the Ekman layer.

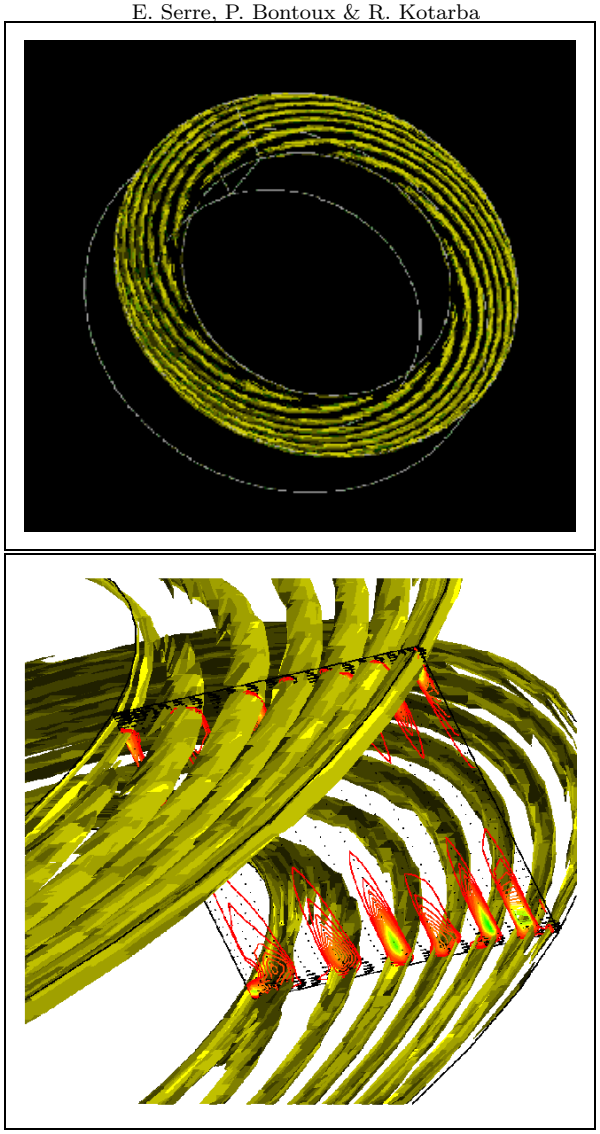

Figure 5. Spiral patterns ($n = 12$ arms) of the Ekman layer instability. Three-dimensional display of iso-surfaces of the axial velocity component in the annular rotating cavity ($R_m = 5$, $L = 3.37$) for $C_w = 530$ and $Re = 1750$. (a) Top: Spiral patterns in the upper Ekman layer; an animation is available on the IJFD website. (b) Spiral patterns in both Ekman layers (yellow), velocity field and contours of positive axial velocity in a ($r$, $z$) meridional plane.

## 4. CONCLUSIONS

The features that are revealed by the DNS investigation are the following:

- The first instability mode is the solution containing axisymmetric rolls (annular patterns). This mode is unstable to a local arbitrarily asymmetric perturbation and

switches to a spiral mode depending on the curvature and on the nature (Ekman or Bödewadt) of the boundary layer.

- In the case of the annular rotor-stator cavity, this spiral mode has a unique wavelength, contrary to Schouveiler's experiments in a cylindrical cavity ($L = 8.75$) which suggested that the spiral mode of instability was limited by a secondary instability of the Eckhaus type. This different behavior during the transition can be explained by a confinement effect. The presence of the shaft and the different aspect ratio conditions can greatly influence the basic state (before transition) and the nature of the transition. Moreover, computations already in progress seem to indicate that the transition in these cavities has been obtained beyond the critical Reynolds number, in a region of the control parameter $Re$ where no phase instability (Eckhaus for example) could be found. Further computations would certainly have to be performed in order to evaluate the occurrence of this kind of instability, particularly in cylindrical cavities more like the experimental apparatus.
- Contrary to the annular rotor-stator case, multiple stable spiral patterns occur in the case of the forced Ekman layer, which seems to indicate a phase instability of the zig-zag type. Computations are already in progress to more accurately determine the nature of this instability. The wavelength of these modes depends on the initial condition (azimuthal wavelength of the disturbance) and does not vary with the curvature.
- In the case of the cylindrical cavity (with no shaft) the Bödewadt layer exhibits two successive spirals, then annular instability patterns following the inward stream that are damped in the vicinity of the axis due to the local Reynolds number which drops below the critical value. A consequence is that the Ekman layer of the rotor is no longer affected by disturbances and remains stable, contrary to the annular case where the disturbances, advected to the rotor layer along the internal shaft, excite a subcritical instability mode inside the Ekman layer.
- From qualitative and quantitative points of view, these patterns are characteristic of the generic type I and type II instabilities of rotating boundary layers. The transition to a three-dimensional mode of instability is quite different in the rotor-stator and the throughflow configurations. When the solution deviates from the axisymmetric pattern to the (multiple) spiral patterns in the rotating cavity, the length and time scales remain comparable in magnitude. In the annular rotor-stator, the bifurcation to the three-dimensional solution corresponds to a transition of a much more complex spatial and temporal behavior.

Our recent results including heat transfer from the wall show substantial changes in the scenario for the first bifurcation between axisymmetric steady, oscillatory, and spiral instabilities. Further studies will extend the investigation to turbulent rotating flows.

## References

1. Caldwell, D.R. and Van Atta, C.W. (1970) Characteristics of Ekman Boundary Layer Instabilities. *J. Fluid Mech.,* **44**, 79–95.
2. Cousin-Rittemard, N., Daube, O., Le Quéré, P. (1998) Sur la Nature de la Première Bifurcation des Ecoulemés Interdisques. *C. R. Acad. Sci. Paris,* Série IIb, **326**, 359–366.
3. Crespo del Arco, E., Maubert, P., Randriamampianina, A. and Bontoux, P. (1996) Spatio-Temporal Behaviour in a Rotating Annulus with a Source-Sink Flow. *J. Fluid Mech.,* **32**, 1–27.

4. Faller, A.J. (1963) An Experimental Study of the Instability of the Laminar Ekman Boundary Layer. *J. Fluid Mech.,* **15**, 560–576.
5. Faller, A.J. and Kaylor, R.E. (1966) Investigations of Stability and Transition in Rotating Boundary Layers. *Dynamics of Fluids and Plasmas,* (S.I. Pai *et al.,* editors), 309–329, Academic Press, New York.
6. Faller, A.J. (1991) Instability and Transition of the Disturbed Flow over a Rotating Disk. *J. Fluid Mech.,* **230**, 245–269.
7. Gauthier, P., Gondret, P. and Rabaud, M. (1999) Axisymmetric Propagating Vortices in the Flow between a Stationary and a Rotating Disk enclosed by a Cylinder. *J. Fluid Mech.,* **386**, 105–127.
8. Greenspan, H.P. (1969) The Theory of Rotating Fluids. Cambridge University Press.
9. Hide, R. (1968) On Source-Sink Flows Stratified in a Rotating Annulus. *J. Fluid Mech.,* **32**, 737–764.
10. Hoffman, N., Busse, F.H. and Chen, W.L. (1998) Transitions to Complex Flows in the Ekman-Couette Layer. *J. Fluid Mech.,* **366**, 311–331.
11. Hoffman, N. and Busse, F.H. (2000) Isolated Solitary Vortex Solutions for the Ekman-Couette Layer. *Eur. J. Mech. B—Fluids*, **19**, 391–402.
12. Itoh, M. (1991) On the Stability of Flow between Coaxial Rotating Disks. *ASME*, Boundary Layer Stability and Transition to Turbulence. FED **114**, 83–89.
13. Lilly, D. K. (1966) On the Instability of Ekman Boundary Flow. *J. Atmos. Sci.,* **23**, 481–490.
14. Owen, J.M. and Rogers, R.H. (1989) Heat Transfer in Rotating Disk Systems. Vol. 1: Rotor-Stator Systems, Ed. W. D. Morris (Wiley, Taunton, Somerset, England).
15. Owen, J.M. and Rogers, R.H. (1995) Heat Transfer in Rotating Disk Systems. Vol. 2: Rotating Cavities, Ed. W. D. Morris (Wiley, Taunton, Somerset, England).
16. San'kov, P.I. and Smirnov, E.M. (1984) Bifurcation and Transition to Turbulence in the Gap between Rotating and Stationary Parallel Disks. *Fluid Dyn.,* **19**(5), 695–702.
17. San'kov, P.I. and Smirnov, E.M. (1991) Stability of Viscous Flow between Rotating and Stationary Disks. *Fluid Dyn.,* **26**(6), 857–864.
18. Savas, O. (1987) Stability of Bödewadt Flow. *J. Fluid Mech.,* **183**, 77–94.
19. Schouveiler, L., Le Gal, P., Chauve, M.P. and Takeda Y. (1996) Experimental Study of the Stability of the Flow between a Rotating and a Stationary Disk. In Advances in Turbulence VI (Gavrilakis S. et al. Eds), 385-388. Kluwer Academic Publishers, Dordrecht.
20. Schouveiler, L., Le Gal, P. and Chauve, M.P. (1998) Stability of a Travelling Roll System in a Rotating Disk Flow. *Phys. Fluids,* **10**, 2695.
21. Schouveiler, L., Le Gal, P., Chauve, M.P. and Takeda Y. (1999) Spiral and Circular Waves in the Flow between a Rotating and a Stationary Disk. *Experiments in Fluids,* **26**, 179–187.
22. Serre, E., Crespo del Arco, E. and Bontoux, P. (1999) Instabilité Tridimensionnelle dans une Cavité de Type Rotor-Stator. *C. R. Acad. Sci. Paris,* Série IIb, **327**, 1139–1146.
23. Serre, E., Hugues, S., Crespo del Arco, E., Randriamampianina, A. and Bontoux, P. (2000) Spiral and Circular Instability Patterns in an Ekman Boundary Layer Flow. *Int. J. Heat Fluid Flows,* **22/1**, 82–93.
24. Serre, E., Crespo del Arco, E. and Bontoux, P. (2001) Annular and Spiral Patterns in a Flow between a Rotating and a Stationary Disk. *J. Fluid Mech.,* **434**, 65–100.
25. Serre, E. and Pulicani, J.P. (2001) A 3D PseudoSpectral Method for Convection in a Rotating Cylinder. *Computers and Fluids*, **30/4**, 491–519.
26. Sirivat, A. (1991) Stability Experiment of Flow between a Stationary and Rotating Disk. *Phys. Fluids,* **A3(11)**, 2664–2671.